Single-molecule studies of disulfide bond reduction pathways used by human thioredoxin

Robert Szoszkiewicz *

Department of Physics, Kansas State University, 307 Cardwell Hall, Manhattan, KS, USA

HIGHLIGHTS

► Large set of AFM data resolves enzymatic catalysis by human thioredoxin directly.
► Single molecule AFM data analyzed by exponential fitting and dwell time histograms.
► Several mechanisms of catalysis, including electron tunneling, are reviewed.
► Novel mode of thioredoxin catalysis is proposed.

GRAPHICAL ABSTRACT
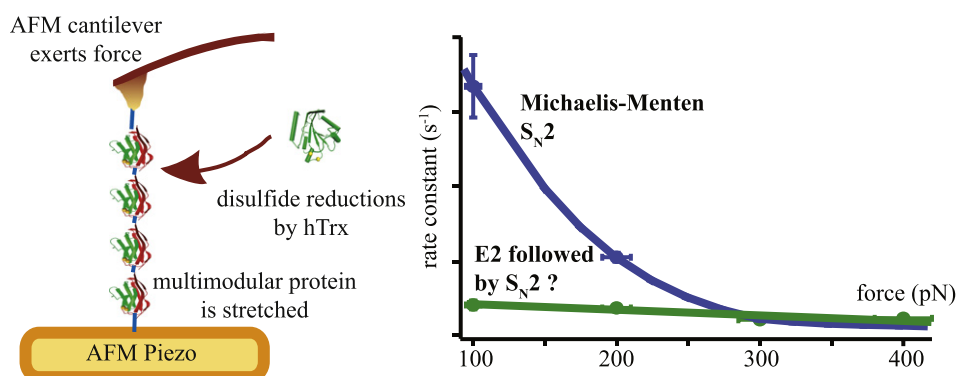
ABSTRACT

Disulfide bond reduction pathways used by human thioredoxin (hTrx) are studied at the single molecule level using a recombinant protein $(I27_{SS})_8$. $(I27_{SS})_8$ contains eight tandem repeats of identical immunoglobulin-like modules with one disulfide bond in each module. Single $(I27_{SS})_8$ molecules are stretched at constant force applied by a cantilever in a force-clamp mode of atomic force microscopy (FC-AFM). Disulfide reduction events are accurately detected from stepwise increases in the end-to-end length of $(I27_{SS})_8$. Earlier FC-AFM studies observed one disulfide reduction pathway used by hTrx and suggested an additional electron tunneling mechanism. Here, a very large set of unbiased FC-AFM data is collected in a range of clamping forces. By analyzing the data using exponential fits and dwell time histograms two disulfide reduction pathways used by hTrx are resolved. Based on previous studies one of these pathways is attributed to force-dependent Michaelis–Menten catalysis. The latter reduction pathway is weakly force-inhibited and occurs sporadically. Bimolecular nucleophilic substitutions (S_N2) and electron tunneling (ET) mechanisms are discussed to explain the second pathway. Direct S_N2 and ET mechanisms cannot be discounted, but a hypothetical E2–S_N2 mechanism involving a hydride reducing a disulfide bond provides an interesting alternative, which needs to be verified in future experiments.

1. Introduction

Enzymatic catalysis outperforms man-made implementations for tightly controlled and stereo-selective chemical reactions with high yields. Molecular details of enzymatic catalysis are still largely unknown.

* Tel.: +1 785 532 0855; fax: +1 785 532 6806.
  E-mail address: szosz@ksu.edu.

Static protein structures, provided by cryo-electron microscopy NMR methods and X-ray crystallography [1–3], do not address enzymatic dynamics. Critical advancements are expected from dynamic NMR methods [4,5] and single molecule methods. For example, recent force-clamp (FC) AFM studies reported on sub-Angstrom enzymatic reconfigurations in force-mediated catalysis of disulfide bond reduction by several kinds of thioredoxins [6,7]. Thioredoxin is a ubiquitous disulfide bond reductase primarily responsible for cell redox homeostasis, anti-apoptotic activity, and signaling [8,9].

The FC-AFM studies of thioredoxin catalyses used a recombinant protein $(I27_{SS})_8$ [6,7,10]. A $(I27_{SS})_8$ molecule contains eight identical modules of the 27th domain from human cardiac titin with precisely one disulfide bond in each module. Each disulfide bond traps a portion of a protein chain, which unfolds after the bond is reduced. $(I27_{SS})_8$ is mechanically clamped between an AFM tip and an arbitrary surface, and reduction events are detected from increases in the protein end-to-end length, i.e., from the FC-AFM length vs. time trace. Using this method, disulfide reduction rate constants were obtained from single exponential fits to the FC-AFM length traces at a given force. In several types of Escherichia coli thioredoxins (TRX) disulfide reduction rate constants initially decreased and then increased as clamping force increased [6,7]. In the case of hTrx, which is structurally similar to E. coli TRX, disulfide reduction rate constants decreased monotonically with force and remained constant above 300 pN [6]. This has been explained by molecular dynamics simulations, which obtained notable differences in width and depth of an enzymatic substrate binding groove as well as different mobilities of a substrate bound to prokaryotic vs. eukaryotic thioredoxins [7]. Furthermore, electron tunneling mechanism was suggested in thioredoxin catalysis [7].

Overall, earlier experimental data and MD simulations found one disulfide reduction pathway in hTrx and suggested an additional electron tunneling mechanism. To verify whether ET is a viable option and to address whether more than one disulfide reduction pathway is used by hTrx a large number of carefully analyzed FC-AFM data is needed.

Methods for the FC-AFM data analysis include exponential fitting to averaged length vs. time FC-AFM traces and dwell time analysis [11,12]. Exponential fitting was applied extensively in ion channel literature [24,25] and FC-AFM studies [6,10]. Dwell time is the time elapsed from presenting a disulfide bond to a reducing environment to an actual bond rupture. Pioneered by Sigworth and Sine in patch clamp studies, dwell time histograms with a square root ordinate vs. logarithm of dwell times display peaks at each rate constant and their errors are distributed evenly for each bin [13–15]. In a previous FC-AFM study, logarithmic dwell time histograms resolved two catalytic pathways for E. coli TRX reducing $(I27_{SS})_8$ at 100 pN clamping force [10].

In this manuscript, disulfide bond reductions by human thioredoxin are addressed using a large number of the FC-AFM data. To compare with previous studies $(I27_{SS})_8$ is used in a range of clamping forces from 100 pN to 400 pN. Rate constants for disulfide bond reductions are obtained from exponential fits and dwell time analysis. The experimental data at 100 pN and 200 pN clamping forces are well fitted using two reaction rate constants, while the data at 300 pN and 400 pN are adequately fitted using one reaction rate constant. Thus, the existence of two disulfide reduction pathways in hTrx is established, and particularly due to the usage of dwell time histograms. One of the pathways is strongly force-inhibited and agrees with previously observed force-dependent Michaelis–Menten type of catalysis by thioredoxins [6,7,10]. The latter pathway is very infrequent and weakly force-inhibited. Direct S_N2 mechanisms and an electron tunneling mechanism are thoroughly discussed to explain the latter pathway. While none of these mechanisms is discounted, they are not very likely in the light of the presented data and literature reports. Instead, a hypothetical $E2$–S_N2 mechanism involving a hydride reducing a disulfide bond provides an interesting alternative, which needs to be verified in future experiments.

2. Materials and methods

2.1. Proteins and enzymes

Expression and purification of $(I27_{SS})_8$ was described in detail previously [16]. QuikChange site-directed mutagenesis using a kit from Stratagene introduced Gly32Cys and Ala75Cys mutations into each I27 module. Multiple rounds of $I27_{G32C-A75C}$ cloning created an N–C linked, eight-domain polyprotein gene of $(I27_{SS})_8$ [17]. This gene was encoded in the vector pQE30 and expressed in the E. coli strain BL21(DE3). The pelleted cells were lysed by sonication and the His6-tagged protein was purified using an immobilized Talon-Co^{2+} column from Clontech followed by gel filtration with Superdex 200 column from GE Healthcare. Purified protein was stored at 4 °C in a buffer of 10 mM HEPES, 150 mM NaCl, 1 mM EDTA, 0.02% NaN3 (w/v), pH 7.2.

Human thioredoxin was purified as described in detail previously [18]. The pACA/hTrx plasmid was expressed in BL21(DE3) cells. Cell pellets were lysed using a French press and stirred with 7% w/v streptomycin sulfate. Protein was precipitated by adding ammonium sulfate to 85% saturation. Crude extracts were applied to a DEAE 52 column equilibrated with 50 mM Tris–HCl, pH 7.5, 1 mM EDTA and 0.1 mM DTT. Thioredoxin was eluted with a NaCl gradient, concentrated, and purified with a Sephadex G-50 column equilibrated with 50 mM Tris–HCl, pH 7.5, 1 mM EDTA and 0.1 mM DTT. Proper fractions were concentrated and further purified using E. coli thioredoxin antibody affinity chromatography. The hTrx concentration was determined spectrophotometrically at 280 nm using a molar extinction coefficient of 8050 M^{-1} cm^{-1}.

For FC-AFM studies a buffer containing 10 μM hTrx, 10 mM HEPES buffer, 150 mM NaCl, 1 mM EDTA, 2 mM NADPH, and 50 nM of eukaryotic thioredoxin reductase from rat liver from Sigma-Aldrich was titrated with 1 M NaOH to pH 7.2. An excess of NADPH and a catalytic amount of thioredoxin reductase were necessary to maintain ~98% of hTrx in an active, reduced form [19,20].

2.2. Force-clamp AFM spectroscopy

A custom built AFM setup [10] with a typical distance resolution in Z-axis of 0.2 nm and feedback time constant of a few ms was used. Commercial V-shaped silicon nitride MLCT-C cantilevers from Bruker, with normal elastic spring constants of 20 pN/nm, were calibrated in liquid prior to each experiment by a thermal method [10,21]. Purified protein was deposited on gold coated glass cover slides from Fisher Scientific.

Data acquisition and data analysis programs were custom developed for Igor Pro 5.0 from Wavemetrics. A following FC-AFM protocol was applied [10]. Initial tip-sample contact was maintained using AFM feedback for 1 s with a contact force of −1 nN. Next, the contact force was reduced to −100 pN and maintained for 100 ms to mark an arbitrary zero extended end-to-end length of $(I27_{SS})_8$. The $(I27_{SS})_8$ molecule was then stretched at 190 pN for 0.15 s in order to quickly expose the disulfide bonds to a bathing solution. Next, a given clamping force was set for 60 s to collect all the reduction events, and not the outliers only. Disulfide bond cleavage was not observed in the absence of hTrx [16]. Any significant changes in the protein end-to-end length occur after the molecule is extended by at least tens of nanometers. Thus, kinetics of disulfide reduction is not expected to depend on water structure on the surface [22], nor on any elasto-adhesive properties of an AFM tip and a substrate [23]. Disulfide reduction events occur after initial $(I27_{SS})_8$ unfolding, so each reduction is spatially isolated by distances of several times the size of a single thioredoxin molecule. This way, the FC-AFM data with long clamping times are unbiased and without any hidden global constraints [24].

2.3. Data analysis

For assessing data fits a standard Pearson (chi-square) test is used; $\chi^2 = \Sigma_i((y_i - f(x_i))/\sigma)^2$, where Σ_i sums over all data points, y_i is an

experimental value at i-th point, $f(x_i)$ is a value of a fitted function at i-th point, and σ is a standard deviation of the fit. To differentiate unambiguously between different models, a standard reduced chi-square, χ^2_{red}, criterion is used. $\chi^2_{red} = \chi^2/(N-c)$, where N is the number of points and c is the number of constraints. A good fit is found if $\chi^2_{red} < 1$.

Statistical bootstrapping yields standard errors of disulfide reduction rate constants obtained by exponential fitting [25]. To do so, a subset of N FC-AFM traces is collected by drawing them with replacements from experimentally collected set of N FC-AFM traces at each given force. Each subset is averaged and fitted with exponentials to obtain reaction rate constants. This procedure is repeated 2000 times to generate a distribution of reaction rate constants. Standard deviation of this distribution is attributed to a standard error of exponential fits at a given force.

Dwell time analysis yields disulfide reduction rate constants from fits to an ordinate y of a logarithmic dwell time histogram. As in Ref. [13]. $y = n_i^{1/2} = (N*\delta x*g(x))^{1/2}$, where n_i is the number of events in i-th bin, N is the total number of events, $x = \ln(t)$ is a logarithmic abscissa, t is time, δx is a bin size, and $g(x)$ is a probability density function; $g(x) = \Sigma_i\ a_i\exp(x + \ln(k_i) + \delta x/2 + \exp(x + \ln(k_i) + \delta x/2))$, where Σ_i sums over fitted reduction rate constants k_i, and a_i is a fraction of N. Using $\sigma = 0.5$ for each bin, χ^2_{red} analysis produced an optimum bin size δx of 0.34 at 100 pN clamping force, and this bin size was also used in other histograms.

3. Results

Fig. 1 shows a schematic FC-AFM setup. Fig. 2 shows that under clamping force $(I27_{SS})_8$ unfolds partially to present disulfide bonds to a bathing solution containing hTrx. At 190 pN clamping force this initial $(I27_{SS})_8$ unfolding yields 10.7 ± 1.1 nm steps in an end-to-end length of the protein. Subsequent disulfide reduction events produce steps from 13.2 ± 1.3 nm at 100 pN to 15.1 ± 1.4 nm at 400 pN. Thus, disulfide reductions in $(I27_{SS})_8$ are easily distinguished from any other events.

Next, disulfide reduction rate constants are obtained using exponential fitting to the reduction parts of FC-AFM length traces, see Fig. 2. First, reduction parts of all FC-AFM length traces at a given clamping force are arranged to begin at an arbitrary zero length and then averaged. Fig. 3 plots the averaged data, which are fitted with single and double exponentials. Exponential fits yield the cumulative time constants τ_i, which are related to cumulative reaction rate constants r_i expressed in s^{-1}: $r_i = 1/\tau_i$. Protein concentration is constant, since only one protein molecule with up to eight disulfide bonds is stretched at a time. This is why r_i are pseudo-first-order rate constants. They are cumulative, since each r_i results from a rate limiting step in a priori unknown series of reactions. These values of r_i are called later "disulfide reduction rate constants". To quantify whether single or double exponential fits are better, fit residuals, χ^2_{red} values, and standard errors of fitted rate constants are compared. See Supplementary materials for details. The results yield that at 100 pN and 200 pN clamping forces two exponential fits are necessary, while at 300 pN and 400 pN single exponential fits are adequate, i.e., single exponentials produce results comparable with double exponential fitting.

In addition, disulfide reduction rate constants are calculated using dwell times of reduction events [10]. Fig. 4 displays logarithmic histograms of sorted dwell times from all FC-AFM length traces at a given clamping force. Logarithmic histograms are fitted with appropriate probability density functions, pdfs. See Materials and methods and Supplementary materials for details. First, rate constants are obtained by fitting pdfs without any assumptions. Next, one rate constant is constrained to be $0.1\ s^{-1}$ across all clamping forces, and the other one is fitted. The value of $0.1\ s^{-1}$ comes from unconstrained fits at 400 pN clamping force, i.e., where disulfide reductions at $0.1\ s^{-1}$ are dominant. Fits to the constrained logarithmic histograms turn out significantly worse than to the unconstrained histograms. This means that a second rate constant must depend on force. The χ^2_{red} analysis and errors of the fitting parameters indicate that two reduction rate constants reproduce the data best at 100 pN and 200 pN clamping forces, while one reduction rate constant produces an adequate fit at 300 pN and 400 pN clamping forces.
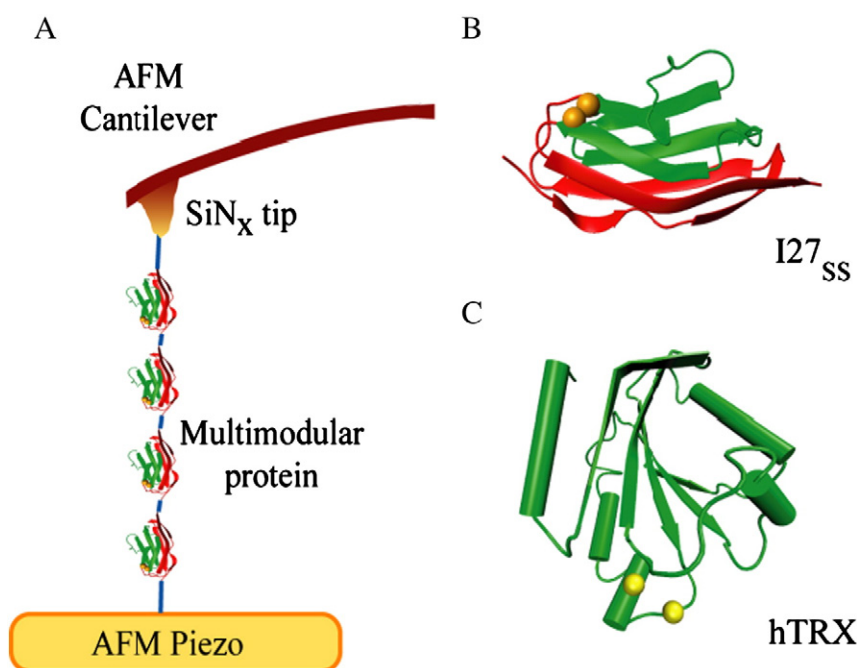

Fig. 1. Experimental schematics. A) In the FC-AFM setup, a cantilever picks up, extends and keeps under a constant force a single molecule. B) Each module of $(I27SS)_8$ is composed of an I27th domain of human cardiac titin (pdb: 1TIT) with one disulfide bond formed between residues 32 and 75 (yellow spheres). The residues in green are mechanically "trapped" behind the disulfide bond, while the residues in red unfold readily under force. C) Human thioredoxin (pdb: 3TRX). Yellow spheres represent α-carbons of catalytic cysteines (Cys 32 and Cys 35) within an enzymatic center.
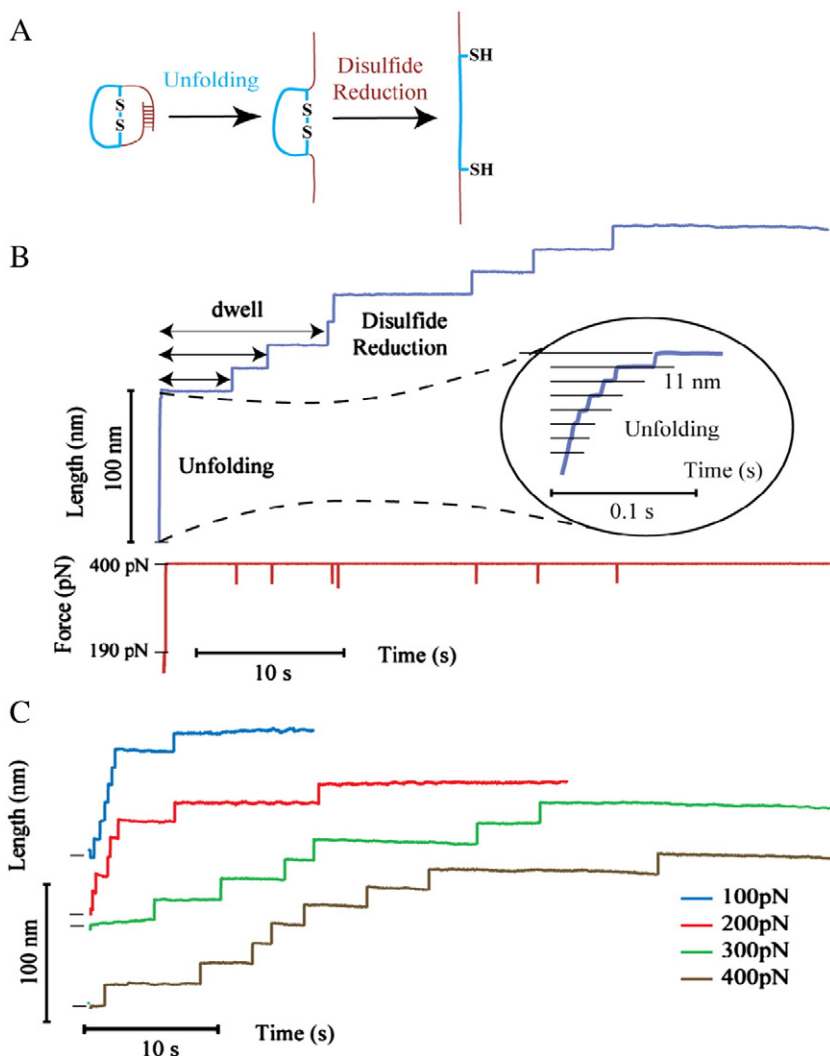
Fig. 2. Sample experimental data. A) Under force, each module of $(I27_{SS})_8$ partially unfolds and exposes its disulfide bonds to a bathing solution. Upon disulfide reduction unfolding of a remaining protein part takes place. B) An FC-AFM length trace measures end-to-end extended protein length vs time. At initial 150 ms at a pulling force of 190 pN the protein extends elastically and partially unfolds. Then, pulling force is changed to an arbitrary value to study kinetics of disulfide bond reductions. The time between the beginning of a disulfide reduction phase and any of the disulfide reduction events is called the dwell time. First three dwell times are marked on a FC-AFM trace. Inset: At least six unfolding steps are resolved. C) A collection of four FC-AFM traces showing only a disulfide reduction phase, i.e., without an initial unfolding part. Each trace was recorded at different pulling forces.

The results from exponential analysis and dwell time histograms agree to resolve two disulfide reduction pathways, called later path A and path B. Disulfide rate constants for path A are 1.67 ± 0.10 s^{-1} at 100 pN and 0.54 ± 0.21 s^{-1} at 200 pN. Disulfide rate constants for path B are 0.20 ± 0.03 s^{-1} at 100 pN and 0.18 ± 0.04 s^{-1} at 200 pN. At 300 pN and 400 pN paths A and B merge into one apparent pathway with rate constants of 0.10 ± 0.01 s^{-1} at 300 pN and 0.12 ± 0.01 s^{-1} at 400 pN. Fig. 5 presents these results.

4. Discussion

Disulfide bond reductions by thioredoxin in ensemble experiments were explained by an S_N2 mechanism [8,19]. The S_N2 mechanism alone, however, was not able explain non-monotonic force dependency of the reaction rate constant observed by FC-AFM in *E. coli* TRX, where two pathways were proposed [6,7].

A predominant disulfide reduction pathway, Path I, found both in *E. coli* TRX and hTRX was explained by a Michaelis–Menten reaction with a force-decelerated catalytic rate constant [6,7]. This mechanism involves initial substrate–enzyme binding followed by actual

catalysis. An initial binding step was found to be much faster than a catalytic step, because prior to catalysis the protein's disulfide bond had to rotate to achieve co-linearity of three sulfur atoms involved in the reaction. Beyond two sulfur atoms forming a disulfide bond, the third atom is one of the two electrons providing sulfur atoms in a thioredoxin catalytic center. As verified by molecular dynamics (MD) simulations, the reaction promoting disulfide bond rotation shortened its length projected upon a pulling axis. Increase of tensile force decreased efficiency of Path I due to an increased difficulty for an enzyme to rotate a disulfide bond at elevated forces.

At elevated clamping forces Path II was proposed to dominate in *E. coli* TRX [6,7]. Path II was explained by a straightforward S_N2 mechanism, which does not involve any canonical substrate–enzyme binding, but occurs via spontaneous collisions of thioredoxin with a stretched protein. Successful collisions are not very frequent, but at increased tensile force a disulfide bond in $(I27_{SS})_8$ is closer to a transition state for its reduction. Recent MD simulations showed that loose protein-thioredoxin associations were likely in *E. coli* TRX due to its shallow substrate binding groove and large substrate mobilities in the groove [7]. However, a substantially deeper substrate binding
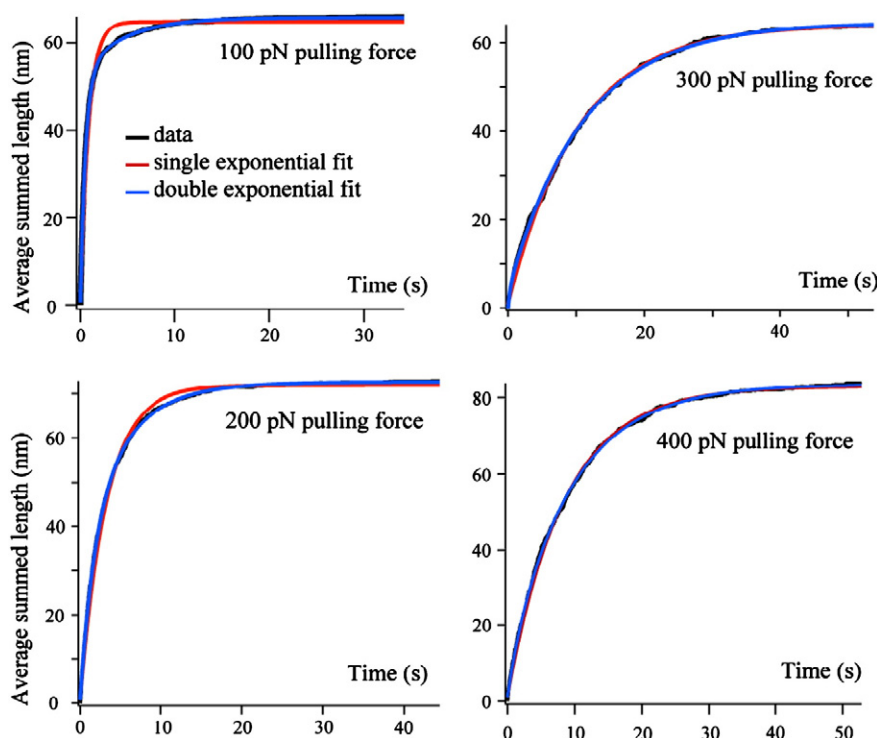
Fig. 3. Analysis of disulfide reductions via exponential fits. Disulfide reduction rates are obtained by fitting single and double exponentials to an averaged FC-AFM length trace obtained after averaging all FC-AFM length traces collected at a given force. Double exponential fits perform well at 100 pN and 200 pN, while single exponential fit is adequate at 300 pN and 400 pN.

groove in hTrx than in *E. coli* TRX would prohibit Path II in hTrx, which agreed with the experimental data [7].

Furthermore, based on non-specific disulfide reductions of $(I27_{SS})_8$ by Zn nanoparticles and its independence on concentration of Zn nanoparticles, a ubiquitous electron tunneling mechanism of disulfide reduction was stipulated to be exercised by all kinds of thioredoxins [7].

Overall, earlier experimental data and MD simulations found one disulfide reduction pathway, Path I, in hTrx, and suggested an additional electron tunneling mechanism. Our experimental results provide a direct experimental evidence for two disulfide reduction pathways, paths A and B, in hTrx, and particularly so by the usage of dwell time histograms.
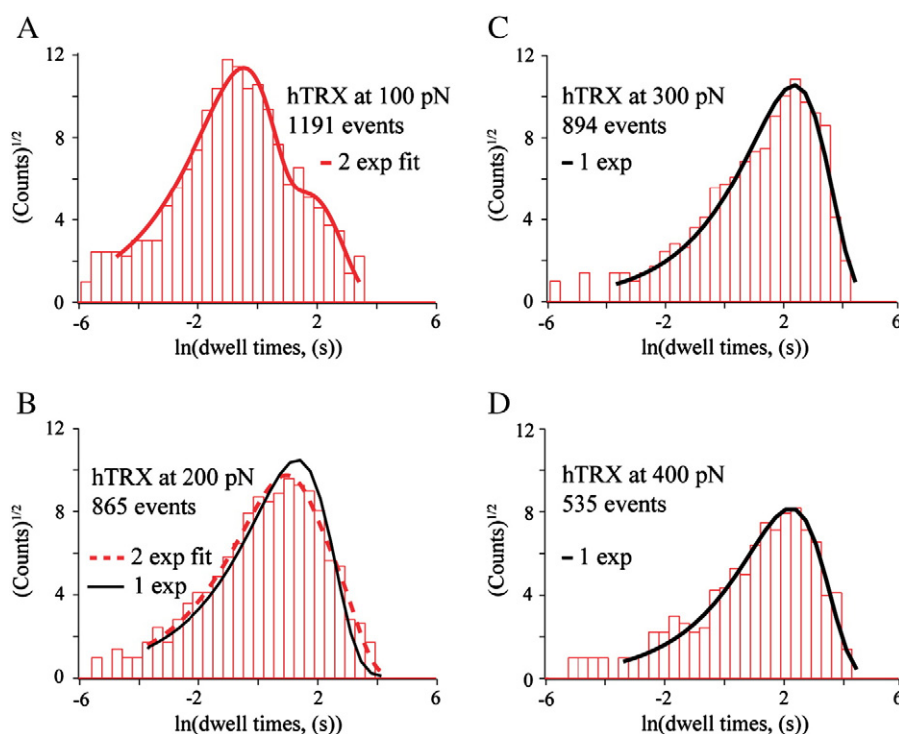

Fig. 4. Dwell time histograms of disulfide reductions. Two processes are well resolvable at 100 pN and 200 pN. One apparent process is adequate at 300 pN and 400 pN.
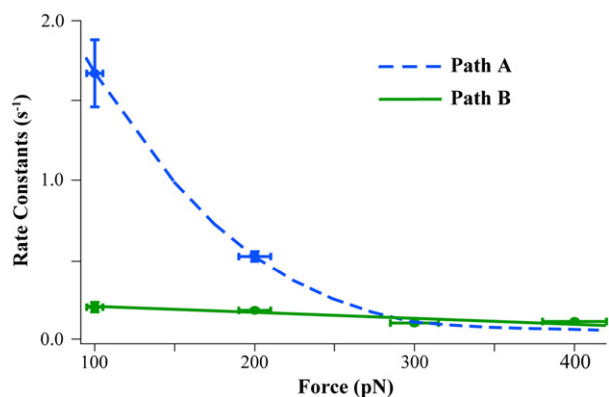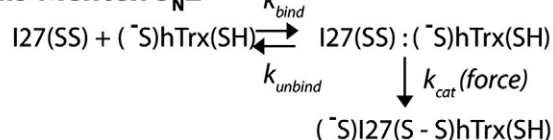
Fig. 5. Disulfide reduction rate constants vs clamping force. Two disulfide reduction pathways, paths A and B, are elucidated from exponential fitting and dwell time analysis.

Scheme 1. Selected reaction schemes for a disulfide bond reduction by hTrx. In a force-dependent Michaelis–Menten disulfide reduction mechanism, which explains path A, k_{bind}, k_{unbind}, and k_{cat} are pseudo-first order reaction rate constants. In a direct S_N2 mechanism, one of the catalytic cysteines in hTrx attacks a disulfide bond to be broken. A pseudo-first order reaction rate constant, k_{02}, is calculated as: $k_{02} = \gamma * [hTrx] * \exp(Force * \Delta x_{02}/(k_B T))$, see text. In a schematic labeled "E2 followed by SN2", see text, a catalytic cysteine from within hTrx does not directly attack a disulfide bond to be broken. The symbols "Cα" and "Cβ" refer to α-carbons and β-carbons in cysteines within I27. The star above one "Cβ" signifies that β-carbons (either ones) are most likely targets for nucleophilic attack from catalytic cysteines within hTrx. After elimination, a hydride attacks the disulfide bond.

To start the data analysis, we note that path A, which is prevalent at 100 pN and 200 pN clamping forces is likely related to Path I from earlier studies, because hTrx and $(I27_{SS})_8$ used by Wiita et al. [6] are used here too. Due to potential differences in enzymatic activity and differences in methodologies between the study of Wiita et al. and a current study, the absolute values of the corresponding rate constants are not compared directly. Instead, to test whether path A and Path I are related, a ratio, R, is calculated, where $R =$ (a rate constant for path A at 100 pN)/(a rate constant of path A at 200 pN). Using current results one gets $R = 3.4 \pm 0.6$ from logarithmic histogram fitting and $R = 3.1 \pm 1.3$ from exponential fits. The model of Wiita et al. yields $R = 3.4 \pm 0.5$. Consequently, path A is attributed to a force-decelerated Michaelis–Menten disulfide reduction pathway, see Scheme 1. Since mechanism details of path A are well established [6,7], mechanistic details of path B are discussed.
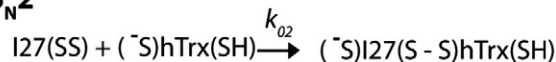
A direct force-dependent pseudo-first order reaction mechanism [6,7] is described by a rate constant k_{02}, which depends on two parameters γ and Δx_{02}, see Scheme 1; γ is a second order rate constant, and Δx_{02} is an averaged distance a disulfide bond must stretch along a reaction coordinate to reach a transition state. For best precision in obtaining γ and Δx_{02} a linear fit to a natural logarithm of k_{02} vs. clamping force is produced, see Suppl. Materials, to yield $\gamma = 24 \pm 7$ nM^{-1}s^{-1} and $\Delta x_{02} = -9 \pm 4$ pm. Thus, using a large number of data acquired in a current study we are able to show that path B is only weakly force-decelerated, i.e., with a small and negative Δx.

Theoretical and experimental single molecule studies of disulfide reductions by small inorganic molecules obtained that a direct mechanism, e.g., a S_N2 mechanism, would produce strongly force-accelerated disulfide reductions with Δx of 30–40 pm, i.e., corresponding to 20% stretching of a $-S-S-$ bond from its initial length of 205 pm to 240 pm at a transition state [6,26]. However, in recent FC-AFM experiments a transition from $\Delta x \sim 40$–50 pm to $\Delta x \sim 5$–15 pm was observed above 500 pN clamping force [27]. Sudden decrease of Δx at elevated clamping forces was interpreted as "cis" to "trans", or "boat" to "chair", conformational switch of a disulfide bond prior to its reduction. Quantum calculations show that a "cis" to "trans" transition extends the disulfide bond by about 10 pm, which brings it closer to a transition state for a subsequent disulfide reduction [27,28]. Furthermore, the "trans" arrangement of $-S-S-$ atoms makes them accessible for an additional "backside" S_N2 disulfide reduction mechanism. While the force range exploited here does not extend to 500 pN, some rare "cis" to "trans" rearrangements of disulfide bonds would be expected to occur at lower forces too. This scenario would account on small values of Δx for the path B, but to the best of the author's knowledge, quantum calculations, e.g., density functional theory calculations, substantiating such a view have not been published yet.
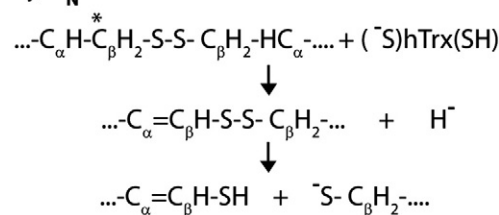
Path B could also relate to electron tunneling [7]. Tunneling involves no bond rupture, no energy barrier, and hence no transition state [29]. There is, however, a reorganization energy barrier is involved in ET, since the system must prepare by obtaining reactive radicals. Here, the ET process is likely to proceed via a thiyl radical ($-S$) in one of the a catalytic cysteines and a subsequent electron transfer to a disulfide bond in $(I27_{SS})_8$. Then, the disulfide reduction itself proceeds via a thiyl radial and a thiolate ($-S^-$) [30]. Formation of a thiyl radial and a thiolate breaks opens the disulfide bond, which is then separated by mechanical force. Using Marcus theory of electron tunneling together with recent derivations of Moser–Dutton and by other authors [31–33] we calculate in detail in the Supplementary materials that tunneling rate constants of the order of 10^3 s^{-1} are expected in the case of a sketched electron tunneling mechanism. Such rate constants of 10^3 s^{-1} are two orders of magnitude larger than what is possible to measure using current FC-AFM setups [36]. Thus, while electron tunneling cannot be excluded, its experimental verification is expected to involve FC-AFM spectrometers with much higher bandwidth.

A hypothetically suitable mechanism of path B could proceed as follows. A bimolecular elimination, E2, is known to compete with an S_N2 mechanism, and particularly in the case of an inaccessible nucleophile. In the most likely E2 scenario a negatively charged sulfur atom from one of the catalytic cysteines would attack a β-carbon in one of the cysteines in a disulfide bond. Similarly to an S_N2 mechanism an E2 mechanism occurs in one step, so at the same time a single bond between an α-carbon and a β-carbon in a cysteine residue becomes a double bond. This is a preferred strategy based on Zaitsev's rule governing E2 reactions, i.e., it creates a more substituted alkene than a terminal S=C− configuration, which would arise from a rupture of a disulfide bond, see Scheme 1. A double bond between an α-carbon and a β-carbon in a cysteine residue requires a hydride, H$^-$, to leave the α-carbon. The other hydrogen would leave in a form of hydron, H$^+$, to form a terminal $-SH$ group in originally attacking catalytic

cysteine of hTrx, see Scheme 1. Hydrides are bad leaving groups due to being strong bases. However, organic chemistry books show many examples of leaving hydrides. For example, hydrides can move between neighboring carbons to generate more stable carbocations. Here, a hydride is hypothesized to be generated by leaving a beta-carbon in one of the cysteines within I27. A hydride is a nucleophile and can attack a disulfide bond to be broken, see Scheme 1. Hydrides, however, are very unstable in solution, so that a subsequent nucleophilic S_N2 attack on a disulfide bond would occur, because the $-S-S-$ bond is only several Ångströms away.

The current data does not warrant any claim of demonstrating any novel disulfide reduction mechanism used by hTrx. Stringent experimental verification, i.e., at different buffers or using isotope effects, is needed. However, there are several advantages of a proposed E2 mechanism with subsequent S_N2-type nucleophilic attack of a hydride on a disulfide bond. First, each β-carbon in cysteine residues within $(I27_{SS})_8$ is surrounded by two hydrogens, and thus quite exposed for a nucleophilic attack by thioredoxin. Second, a hydride is small and a disulfide bond is easily accessible for it. Third, this mechanism explains small, force-decelerated, rate constants. This is because any nucleophilic attack of H^- on a sulfur atom in a disulfide bond becomes less probable when bonds are elongated. Probability of this process depends on a volume, which a hydride needs to explore before reaching a sulfur atom. Excluding any electrostatic guiding [37], this volume is a sphere with a radius r_{HtoS}, i.e., a distance between hydrogen at an α-carbon and its nearest sulfur atom in a disulfide bond to be broken. Supposing ~10% increase in r_{HtoS}, when force changes from 100 pN to 400 pN, one obtains about 30% decrease in the rate constant, which explains the experimental data. While 10% r_{HtoS} increase of r_{HtoS} is reasonable based on MD simulations of a disulfide bond stretching [6,26,27], the E2–S_N2 mechanism is currently only a possibility, which needs to be verified using further studies. Please note, however, that path A is equally elaborated, since it requires twisting of a disulfide bond before reducing it.

Finally, potential conformational flexibility of hTrx might relate to mechanistic subtleties. By using available structural data of TRX bound to three different polypeptides Wiita et al. [6], obtained via molecular dynamics simulations distinctively different reaction rate constants for path A in the case of each peptide. Different reaction rates were associated with different binding ways of each peptide. Any statistically justifiable spread in binding conformations between hTrx and a disulfide bond embedded within I27 should result in a small spread of obtained reaction rates. In all single molecule assays with thioredoxin, however, a bimodal distribution of rates is observed [6,7,10]. Thus, thioredoxin–peptide conformations seem to be quite unique for each system.

5. Conclusions

Due to a low reduction potential of thiols and their ease to be oxidized to sulfur species, disulfide chemistry is very rich, which can wreak havoc in tightly spaced cellular compartments if not properly controlled [7,34,35,37,39]. Through deeper binding groove and stronger substrate binding than *E. coli* analogs, human thioredoxin has evolved to achieve substantial enhancement of one major disulfide reduction pathway, and marginalization of other competing pathways [7]. This is a good strategy to enhance specificity of an enzyme. The FC-AFM studies at high clamping forces, however, are able to reveal marginalized disulfide reduction pathways.

Using a large set of FC-AFM data catalytic behavior of human thioredoxin in a force range between 100 pN to 400 pN was analyzed here. Fits to an ensemble average of all FC-AFM length traces and dwell time histograms at a given force yielded disulfide reduction rate constants. This way two distinctive disulfide reduction pathways, A and B, were directly resolved. The paths A and B reflect dynamic variability of hTx enzymatic activity, which becomes experimentally accessible only when lots of experimental data is collected and analyzed with several data analysis methods.

Based on agreement between our results and previously published studies, path A was attributed to the Michaelis–Menten catalysis. The second, much less frequent, reaction pathway showed to be very weakly force dependent. Three possible mechanisms for path B were carefully discussed: a straightforward S_N2 mechanism, electron tunneling, and a combination of E2 with subsequent S_N2 attack by a hydride. Direct S_N2 and ET mechanisms cannot be discounted, but a currently hypothetical E2–S_N2 mechanism provides an interesting alternative to explain the experimental data. However, stringent experimental verifications are needed, i.e., by using different buffers or isotope effects, to warrant such a E2–S_N2 mechanism.

Acknowledgments

Appendix A. Supplementary data

Supplementary data to this article can be found online at http://dx.doi.org/10.1016/j.bpc.2013.01.002.

References

[1] D.A. Kraut, K.S. Carroll, D. Herschlag, Annual Review of Biochemistry 72 (2003) 517–571.
[2] S. Hammes-Schiffer, S.J. Benkovic, Annual Review of Biochemistry 75 (2006) 519–541.
[3] U.B.S. Rawat, A.V. Zavialov, J. Sengupta, M. Valle, R.A. Grassucci, J. Linde, B. Vestergaard, M. Ehrenberg, J. Frank, Nature 421 (2003) 87–90.
[4] K.A. Henzler-Wildman, M. Lei, V. Thai, S.J. Kerns, M. Karplus, D. Kern, Nature 450 (2007) 913–927.
[5] J. Villali, D. Kern, Current Opinion in Chemical Biology 14 (2010) 636–643.
[6] A.P. Wiita, R. Perez-Jimenez, K.A. Walther, F. Grater, B.J. Berne, A. Holmgren, J.M. Sanchez-Ruiz, J.M. Fernandez, Nature 450 (2007) 124–130.
[7] R. Perez-Jimenez, J.Y. Li, P. Kosuri, I. Sanchez-Romero, A.P. Wiita, D. Rodriguez-Larrea, A. Chueca, A. Holmgren, A. Miranda-Vizuete, K. Becker, S.H. Cho, J. Beckwith, E. Gelhaye, J.P. Jacquot, E.A. Gaucher, J.M. Sanchez-Ruiz, B.J. Berne, J.M. Fernandez, Nature Structural & Molecular Biology 16 (2009) 592–599.
[8] E.S. Arner, A. Holmgren, European Journal of Biochemistry 267 (2000) 6102–6109.
[9] A. Holmgren, Annual Review of Biochemistry 54 (1985) 237–271.
[10] R. Szoszkiewicz, S.R.K. Ainavarapu, A.P. Wiita, R. Perez-Jimenez, J.M. Sanchez-Ruiz, J.M. Fernandez, Langmuir 24 (2008) 1356–1364.
[11] D.R. Cox, H.D. Miller, The theory of stochastic processes. Editor, Methuen, London, 1965.
[12] O.P. Hamill, A. Marty, E. Neher, B. Sakmann, F.J. Sigworth, Pflugers Archiv—European Journal of Physiology 391 (1981) 85–100.
[13] F.J. Sigworth, E. Neher, Nature 287 (1980) 447–449.
[14] R.W. Aldrich, D.P. Corey, C.F. Stevens, Nature 306 (1983) 436–441.
[15] F.J. Sigworth, S.M. Sine, Biophysical Journal 52 (1987) 1047–1054.
[16] A.A. Carter, R.E. Oswald, Journal of Neuroscience Methods 60 (1995) 69–78.
[17] R.E. Wachtel, Journal of Neuroscience Methods 25 (1988) 121–128.
[18] A.P. Wiita, S.R.K. Ainavarapu, H.H. Huang, J.M. Fernandez, Proceedings of the National Academy of Sciences of the United States of America 103 (2006) 7222–7227.
[19] M. Carrion-Vazquez, A.F. Oberhauser, S.B. Fowler, P.E. Marszalek, S.E. Broedel, J. Clarke, J.M. Fernandez, Proceedings of the National Academy of Sciences of the United States of America 96 (1999) 3694–3699.
[20] X.L. Ren, M. Bjornstedt, B. Shen, M.L. Ericson, A. Holmgren, Biochemistry 32 (1993) 9701–9708.
[21] H.J. Butt, B. Cappella, M. Kappl, Surface Science Reports. 59 (1–6) (2005) 1–152.
[22] T.D. Li, J.P. Gao, R. Szoszkiewicz, U. Landman, E. Riedo, Physical Review B 75 (2007) 115415.
[23] R. Szoszkiewicz, A.J. Kulik, G. Gremaud, M. Lekka, Applied Physics Letters 86 (2005) 123901.
[24] D.A. Koster, C.H. Wiggins, N.H. Dekker, Proceedings of the National Academy of Sciences of the United States of America 103 (2006) 1750–1755.
[25] B. Efron, The Jackknife, the Bootstrap, and Other Resampling Plans. Editor, S.I.A.M., Philadelphia, PA, 1982.
[26] P.A. Fernandes, M.J. Ramos, Chemistry—a European Journal 10 (2004) 257–266, http://dx.doi.org/10.1002/chem.200305343.

[27] S. Garcia-Manyes, J. Liang, R. Szoszkiewicz, T.L. Kuo, J.M. Fernandez, Nature Chemistry 1 (2009) 236–242.
[28] D. Jiao, M. Barfield, J.E. Combariza, V.J. Hruby, Journal of the American Chemical Society 114 (1992) 3639–3643.
[29] R.A. Marcus, Pure and Applied Chemistry 69 (1997) 13–29.
[30] C.S. Sevier, C.A. Kaiser, Nature Reviews Molecular Cell Biology 3 (2002) 836–847.
[31] C.C. Page, C.C. Moser, X.X. Chen, P.L. Dutton, Nature 402 (1999) 47–52.
[32] A.A. Voityuk, The Journal of Physical Chemistry. B 115 (2011) 12202–12207.
[33] C.C. Moser, J.M. Keske, K. Warncke, R.S. Farid, P.L. Dutton, Nature 355 (1992) 796–802.
[34] H.B. Gray, J.R. Winkler, Quarterly Reviews of Biophysics 36 (2003) 341–372.
[35] Z.Y. Cheng, J.F. Zhang, D.P. Ballou, C.H. Williams, Chemical Reviews 111 (2011) 5768–5783.
[36] A. Dey, R. Szoszkiewicz, Nanotechnology 23 (2012) 175101.
[37] I.T. Suydam, C.D. Snow, V.S. Pande, S.G. Boxer, Science 313 (2006) 200–204.
[38] N.M. Giles, G.I. Giles, C. Jacob, Biochemical and Biophysical Research Communications 300 (2003) 1–4.
[39] G.I. Giles, C. Jacob, Biological Chemistry 383 (2002) 375–388.